International Journal of Nanomedicine

Dovepress
open access to scientific and medical research

Open Access Full Text Article

ORIGINAL RESEARCH

Using ferromagnetic nanoparticles with low Curie temperature for magnetic resonance imaging-guided thermoablation

This article was published in the following Dove Press journal:
International Journal of Nanomedicine
8 August 2016
Number of times this article has been viewed

Vít Herynek[1]
Karolína Turnovcová[2]
Pavel Veverka[3]
Tereza Dědourková[4,5]
Pavel Žvátora[6]
Pavla Jendelová[2]
Andrea Gálisová[1]
Lucie Kosinová[7]
Klára Jiráková[2]
Eva Syková[2]

[1]MR-Unit, Radiodiagnostic and Interventional Radiology Department, Institute for Clinical and Experimental Medicine, Prague, [2]Department of Neuroscience, Institute of Experimental Medicine, [3]Department of Magnetics and Superconductors, Institute of Physics, Czech Academy of Sciences, Prague, [4]Department of Inorganic Technology, Faculty of Chemical Technology, University of Pardubice, [5]SYNPO, akciová společnost, Pardubice, [6]Department of Analytical Chemistry, Institute of Chemical Technology, [7]Diabetes Center, Institute for Clinical and Experimental Medicine, Prague, Czech Republic

Correspondence: Vít Herynek
MR-Unit, Radiodiagnostic and Interventional Radiology Department, Institute for Clinical and Experimental Medicine, Vídeňská 1958/9, 14021 Prague 4, Czech Republic
Tel +420 261 362 703
Fax +420 241 728 224
Email vit.herynek@medicon.cz

Introduction: Magnetic nanoparticles (NPs) represent a tool for use in magnetic resonance imaging (MRI)-guided thermoablation of tumors using an external high-frequency (HF) magnetic field. To avoid local overheating, perovskite NPs with a lower Curie temperature (T_c) were proposed for use in thermotherapy. However, deposited power decreases when approaching the Curie temperature and consequently may not be sufficient for effective ablation. The goal of the study was to test this hypothesis.

Methods: Perovskite NPs (T_c=66°C–74°C) were characterized and tested both in vitro and in vivo. In vitro, the cells suspended with NPs were exposed to a HF magnetic field together with control samples. In vivo, a NP suspension was injected into a induced tumor in rats. Distribution was checked by MRI and the rats were exposed to a HF field together with control animals. Apoptosis in the tissue was evaluated.

Results and discussion: In vitro, the high concentration of suspended NPs caused an increase of the temperature in the cell sample, leading to cell death. In vivo, MRI confirmed distribution of the NPs in the tumor. The temperature in the tumor with injected NPs did not increase substantially in comparison with animals without particles during HF exposure. We proved that the deposited power from the NPs is too small and that thermoregulation of the animal is sufficient to conduct the heat away. Histology did not detect substantially higher apoptosis in NP-treated animals after ablation.

Conclusion: Magnetic particles with low T_c can be tracked in vivo by MRI and heated by a HF field. The particles are capable of inducing cell apoptosis in suspensions in vitro at high concentrations only. However, their effect in the case of extracellular deposition in vivo is questionable due to low deposited power and active thermoregulation of the tissue.

Keywords: perovskite nanoparticles, hyperthermia, high-frequency magnetic field, MRI, tumor ablation

Introduction

Magnetic nanoparticles (NPs) represent an interesting tool for use in magnetic resonance imaging (MRI)-guided thermoablation, using an external high-frequency (HF) magnetic field. It may represent a complementary oncological treatment.[1,2] Tumor cells are known to be more sensitive to heat than healthy tissue. Due to the pathologic blood vessels, the thermal elevation persists inside the tumor, whereas neighboring normal tissues, adequately perfused, are cooled.[3] Therefore, exposing the tissue to temperatures between 42°C and 45°C may lead to destruction of the tumor cells whereas the healthy ones survive. The concept of the treatment is based on depositing magnetic NPs in the vicinity of the tumor and their subsequent heating by an external alternating magnetic field.[4–7]

submit your manuscript | www.dovepress.com
Dovepress
http://dx.doi.org/10.2147/IJN.S109582

The heating is caused by magnetic losses, either by the rotation of magnetic moments[8] in the case of superparamagnetic particles or by hysteresis losses[9] in the case of ferro- or ferrimagnetic particles. Also, frictional losses due to rotational Brownian motion in the carrier liquid can contribute to the total effect. Various aspects of the method have already been widely discussed.[10]

The effectiveness of heating depends on many aspects. Besides modulating the parameters of the applied alternating magnetic field (eg, field amplitude and frequency), a suitable adjustment of the core properties is important. This concerns magnetization and coercivity, thus providing a reasonable heating efficiency, and a Curie temperature (T_c), above which the material becomes paramagnetic and hysteresis losses become zero. By adjusting the Curie temperature slightly above the therapeutic temperature (~45°C), one can achieve a self-controlled heating mechanism and avoid overheating the tissue.[11]

Preparation of suitable particles represents a particularly challenging problem. One possible approach is the use of complex magnetic oxides as core materials, whose magnetic properties can be properly tailored in various ways, such as modifying the intrinsic properties depending on the composition and structure or modifying the extrinsic properties (eg, particle size and size distribution). Simultaneously, attention should be paid to the quality of the coating, ensuring stability of the suspension and biocompatibility with respect to potential medical applications. These possibilities were discussed with several examples by Pollert et al,[12] where the position of $La_{1-x}Sr_xMnO_3$ (LSMO) perovskites, offering exceptional feasibility, was stressed.

While there are limited possibilities to control the extent of the lesion in the case of ferromagnetic materials, NPs with a lower Curie temperature can be used to avoid overheating. However, deposited power decreases when approaching the Curie temperature and consequently may not be sufficient for effective ablation.

Distribution of the NPs may be easily controlled by MRI. The imaging method is based on the spatially resolved detection of protons. As water in the tissue contains most of the protons, MRI in fact detects the distribution of tissue water. However, MRI contrast can also be weighted by different physical properties of the detected water molecules, the most important of which are the so-called relaxation times T_1, T_2, or T_2*. Although MRI does not detect the NPs themselves, magnetic NPs create local inhomogeneities in a static field leading to the considerable shortening of T_2 and T_2* relaxation times of water and rapid signal loss. The presence of magnetic NPs in the tissue is therefore manifested by hypointense areas in T_2-weighted or T_2*-weighted MR images. The size of the area impacted by a superparamagnetic or ferromagnetic contrast agent is usually considerably larger than the size of the contrast agent itself.

The goals of this study was to test perovskite NPs with low T_c, as an MRI contrast agent, and study the conditions at which they are capable of inducing thermoablation.

Methods

Synthesis of NPs

Based on our previous experiments, manganese perovskite $La_{1-x}Sr_xMnO_3$ NPs (where x=0.25–0.35) were prepared according to the following protocol described in part in Pollert et al.[13,14] Stoichiometric La_2O_3 calcined at 1,000°C was used as the source of La, whereas $SrCO_3$ and $MnCO_3$ with chemically determined metal content were used as the other starting materials. The corresponding amounts of La_2O_3 (13 mmol) and $SrCO_3$ (7 mmol) were mixed and slowly decomposed by HNO_3, whereas the decomposition of $MnCO_3$ (20 mmol) was carried out separately and led to the formation of brown precipitates that were subsequently dissolved upon addition of a few drops of H_2O_2. The solutions were combined and citric acid monohydrate (60 mmol) diluted in 20 mL of water was added. Ammonia was used to adjust the pH to 7.6 and ethylene glycol (90 mmol) was added. The mixture was heated to 85°C while stirring. After gelification had occurred, the material was slowly dried by gradual increase of temperature. Further heating led to burning of organic components at approximately 220°C. The material was thoroughly homogenized and calcined at 400°C for 4 hours. The subsequent thermal treatment at 775°C for 3 hours in air provided a single-phase manganese perovskite crystallites of a mean size 30 nm (the as-grown LSMO product). The final NPs containing crystallites of a mean size of 21 nm were obtained by three cycles of rolling on a simple rolling machine followed by mixer milling in ethanol at 21 Hz on a Retsch MM 301 mill (Retsch GmbH, Haan, Germany) equipped with a 25-mL stainless steel vessel and 15-mm ball.

Manganite perovskite NPs were covered by a continuous layer of the hydrated silica oxide during an encapsulation procedure that consists of the treatment of the surface of the synthesized grains by nitric acid, subsequent stabilization of the suspension by ammonium citrate, and coating by the hydrated silica oxide in a medium of water, ethanol, and ammonia at 57°C for 4 hours and followed by slow cooling

to room temperature under mechanical stirring employing tetraethoxysilane. Finally, in order to get NPs of required size, the product was subjected to a separation procedure via centrifugation.[15]

Characterization

The phase composition and the crystallite size of the NPs were determined using a Bruker D8 powder diffractometer (CuKα radiation, Scintilation detector; Bruker, Karlsruhe, Germany). X-ray diffraction patterns were analyzed by the Rietveld method in FULLPROF (J Rodriguez-Carvajal, FULLPROF, version 4.30) using the data from Inorganic Crystal Structure Database (ICSD, version 2008). The crystallite size delimited X-ray diffraction coherence length and thus contributed to peak width. Thompson-Cox-Hastings pseudo-Voigt profile was used to resolve instrumental strain and size contributions to peak-broadening. Instrumental resolution was determined by measuring strain-free tungsten powder with a crystallite size of 9.4 μm.

The static magnetic properties of both bare and silica-coated LSMO NPs were studied using a SQUID magnetometer Quantum Design MPMS-5S (LOT-QuantumDesign GmbH, Darmstadt, Germany). The Curie temperature T_c was determined as the inflection point on the curve describing the dependence of the susceptibility to temperature.

The size and shape of the NPs were directly observed by a transmission electron microscope Philips CM120, 120 kV, LaB_6 (Philips, Amsterdam, the Netherlands).

The hydrodynamic diameter of LSMO@SiO_2 was determined on the basis of Dynamic Light Scattering using Photon Cross Correlation Spectroscopy NANOPHOX (Sympatec, Clausthal-Zellerfeld, Germany) that suppresses multiple scattering.

Relaxometry

Magnetic resonance relaxation time measurements were carried out on a 0.5 T Bruker Minispec MQ20 relaxometer (Bruker BioSpin, Rheinstetten, Germany) to characterize the particles and their impact on a contrast in MR images. A standard Carr-Purcell-Meiboom-Gill (CPMG) sequence (echospacing 2 ms, number of echoes varied between 500 and 2,000, recovery time TR = 5,000 ms, eight acquisitions) was used.

Relaxivity r_2 of the NPs was calculated as reciprocal values of the relaxation time T_2 related to Mn concentration (c) according to the formula:

$$r_2\ (s^{-1}\ mM^{-1}) = 1/T_2/c$$

The contribution of the liquid media was negligible and therefore disregarded.

Magnetic heating apparatus

The apparatus assembled in our laboratory consisted of a generator, power amplifier, and a water-cooled tuned excitation coil with an inside probe diameter of 80 mm. For in vitro measurements, a cylindrical inset made of polystyrene foam was inserted into the coil as thermal insulation and the samples were placed in the hole in the inset. Temperature was measured by an optic fiber thermometer connected to a computer. The magnetic field in the coil was measured by a single-loop coil placed on the inside surface of the probe and connected to a measurement device. Details of the apparatus and additional factors of calorimetric measurements were described by Kaman et al[15] and Veverka et al.[16] Magnetic heating experiments were performed using an alternating field with the following parameters: frequency f =480 kHz and magnetic field H_{max} =11 mT.

Cells

We used rat mesenchymal stem cells (rMSC) from bone marrow (BM-MSCs) or from adipose tissue (AT-MSCs), and rat glioblastoma cells, cell line C6, throughout the study. BM-MSCs from Wistar rats were isolated from rat bone marrow as described elsewhere.[17] Briefly, bone marrow from 14-day-old rat femurs and tibias was washed out, placed on a 10 cm^2 Petri dish, and nonadherent cells were removed after 72 hours.

AT-MSCs from transgenic Lewis rats were isolated from the visceral adipose tissue according to Fabryova et al.[18] Briefly, tissue was digested by collagenase, filtered, overlayered on 5 mL of Ficoll 1,077 g/mL (Ficoll-Paque Premium; GE Healthcare Bio Science AB, Upsala, Sweden) and spun. The cells in the interphase were collected and seeded in a tissue flask.

Rat glioma cell line C6 (ATCC® CCL-107™) was obtained from Cestmir Altaner, Institute of Experimental Oncology SA, Bratislava, Slovakia.

The cells were cultivated with changing media twice per week and passaged when having reached 90% confluence.

In vitro test of local hyperthermia

Four cell samples containing 1 million cells were prepared for each experiment. Two cell samples were mixed with highly concentrated NP suspension (the final NP concentration was c=16 mM [Mn]).

One sample with NPs and one sample with clean cells were exposed to a HF magnetic field (480 kHz, 11 mT, 60 minutes). A cuvette (diameter 10 mm) with the sample was insulated by an 8 cm polystyrene cylinder during exposition. The other two samples were used as control samples; they were laid on a bench at the same temperature as the samples exposed to the HF field during the experiment. The cells were counted and a viability test was performed to determine the effect of hyperthermia after the HF field exposure and in the control samples.

Cell viability was measured immediately after thermoablation and after 24 hours. The NPs were left in the cell suspension during this period. Cell viability was determined by using the Trypan blue exclusion test, which can determine the number of viable cells present in a cell suspension. Cells were counted manually in the Burker chamber under a light microscope. Cell viability of rMSC and C6 was also verified by automated cell counting systems, flow cytometer BD FACSAria (Becton Dickinson, San Diego, CA, USA), and Apogee A-50 Micro (Apogee Flow System, Hemel Hempstead, Hertfordshire, UK). All the cell samples were handled in the same way during this experiment.

Test of local hyperthermia in vivo

The experiment consisted of several steps:

1. Implanting the tumor cells in the experimental animals.
2. MRI monitoring of the tumor growth.
3. Injection of NPs.
4. Verifying the NP distribution using MRI.
5. In vivo hyperthermia.
6. Histology evaluation of the affected tissue.

Tumor model: 2 million rat glioblastoma cells (line C6) were implanted subcutaneously to the back (ten experimental rats Brown-Norway) or into the muscle of the hind leg (four rats).

NP application: suspension (50 µL, 55 mM [Mn]) was injected directly into the tumor ~2 weeks after cell implantation. The time interval between C6 cell implantation and NP application slightly differed for each group of animals depending on the tumor growth. The application and subsequent treatment was performed when the longest diameter of the tumor reached 10 mm (measured on MR images).

MRI guidance: MR images were obtained using a 4.7 T Bruker imager (Bruker BioSpin) equipped with an in-house-made surface transmit–receive coil. The rats were anesthetized by passive inhalation of isoflurane (Isofluran; Torrex Chiesi Pharma, Vienna, Austria) in air (5% for anesthesia induction, 1.5%–2% for maintenance). Breathing was monitored during the measurements. Single sagittal, coronal, and transversal images were obtained by a fast gradient-echo sequence to localize the subsequent T_2-weighted images, as measured by a standard turbo spin-echo sequence. The sequence parameters were: repetition time TR =3,000 ms, effective echo time =36 ms, turbo factor =8, number of acquisitions =4, field of view =4 cm, matrix = 256×256, slice thickness =0.75 mm, and slice separation =0.75 mm. Both sagittal and transversal images were obtained. The same measurement protocol was used for both the injection sites.

After MRI, an optical fiber with a fluorescent probe was inserted through a catheter into the tumor to monitor the temperature. The rats were placed (without waking them up) into the probe of the magnetic heating apparatus and exposed to a HF field (480 kHz, 11 mT) for up to 60 minutes.

The temperature in the tumor was recorded each 0.25 seconds using a personal computer and averaged. The animals were sacrificed 1 day after ablation. Animals were anesthetized using 5% isoflurane before intracardiac perfusion with 4% paraformaldehyde phosphate-buffered to pH 7.4. Extirpated tumors were postfixed overnight in the same fixative solution and cryoprotected with 30% sucrose for 48 hours. Approximately 40-µm thick slices were then processed for terminal deoxynucleotidyl transferase dUTP nick end labeling (TUNEL; Abcam, Cambridge, UK) and active caspase-3 expression (Sigma-Aldrich Co., St Louis, MO, USA).

Altogether six animals with tumor were subjected to NP injection directly into the tumor and to thermoablation in the HF magnetic field. Control animals with tumors underwent either HF field exposure without NPs (four rats), or application of NPs without exposure to HF field (three rats) to eliminate both the influence of the HF field or NPs themselves.

The course of the temperature evolution in the tumor during ablation was fitted by a polynomial curve (third order). The polynomial parameters calculated for the group of animals treated by HF field with and without NPs were compared by a nonparametric Mann–Whitney *U*-test as well as single minute average values of the actual temperature. Statistical evaluation was not performed on the group of rats with the tumor in the muscle of the hind leg due to low numbers of animals. Statistical evaluation of apoptotic cell counts was not performed due to negligible number of apoptotic cells in the tumor tissue (see Results and discussion, Histology section).

The use of animals in this study was approved by the Ethics Committee of the Thomayer Hospital and Institute for Clinical and Experimental Medicine (Prague, Czech Republic) and by the Ministry of Health of the Czech

Table 1 Structural data of bare samples of manganese perovskites LSMO according to XRD

Batch no	Composition (x)	Mean LSMO core size d_{XRD} (nm)	a (nm), mean (SD)	c (nm), mean (SD)	Mn-O (nm), mean (SD)	O-Mn-O (degrees), mean (SD)	Mn-O-Mn (degrees), mean (SD)	V/z (10^{-3} nm^3), mean (SD)
I	0.25	32	0.55048 (2)	1.33578 (8)	0.1951 (10) [6×]	89.3 (8) [6×], 90.7 (8) [6×]	167.9 (11)	58.42 (1)
II	0.30	27	0.54993 (3)	1.33556 (12)	0.1948 (13) [6×]	89.4 (9) [6×], 90.6 (9) [6×]	168.8 (13)	58.30 (1)
III	0.35	22	0.54946 (3)	1.33584 (12)	0.1947 (10) [6×]	89.4 (7) [6×], 90.6 (7) [6×]	168.6 (10)	58.21 (1)

Notes: d_{XRD} is the mean size of crystallites, the hexagonal setting is used for the $R\bar{3}c$ structure, V/z is the unit cell volume per formula unit. Numbers in the square brackets represent the number of replications in the crystal structure.
Abbreviations: LSMO, $La_{1x}Sr_xMnO_3$; XRD, X-ray diffraction; SD, standard deviation of the last digit.

Republic. All animals were kept and handled according to the European Convention on Animal Care.

Results and discussion

We tested three types of LSMO NPs with certain modifications that may influence their intrinsic properties.[19] Structure data of the bare products are provided in Table 1. X-ray diffraction patterns revealing rhombohedral structure with space group $R\bar{3}c$ of the three tested products are shown in Figure 1. The transmission electron microscopy analysis (Figure 2) indicated a relatively narrow size distribution of the encapsulated NPs and a suppressed tendency to irreversible agglomeration. Table 2 summarizes mean diameters of magnetic cores, whole silica-coated NPs, and silica shell thickness evaluated from transmission electron microscopy images. Histograms showing size distribution of the silica-coated NPs are in Figure 3. Variations in core composition and silica thickness layer resulted in small variations in magnetization and Curie temperature (Table 3).

The NPs possessed high relaxivity r_2, which is crucial for MR imaging. At 0.5 T relaxivity r_2 in diluted samples was 302 s^{-1}/mM (Mn) (23°C) or 225 s^{-1}/mM (Mn) (37°C) for the product III with the smallest core.

Relaxivity was strongly dependent on temperature due to low Curie temperature (Figure 4). Relaxivity values exceeded that of standard iron oxide NPs (reaching 126–213 s^{-1}/mM [Mn] depending on the coating[20,21]). Relaxivity of

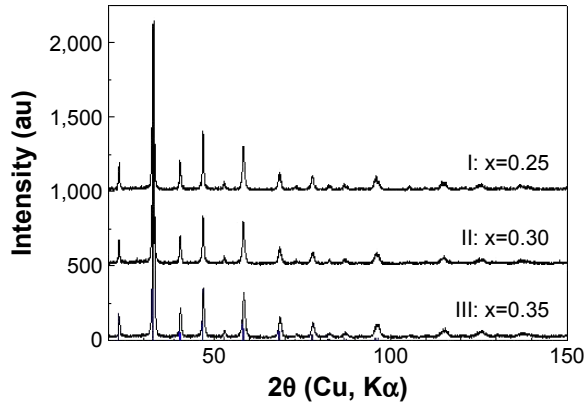

Figure 1 X-ray diffraction patterns of $La_{1-x}Sr_xMnO_3$ (x=0.25, 0.30, and 0.35) revealing rhombohedral structure with space group $R\bar{3}c$.
Note: Blue diffraction lines corresponding to the manganese perovskite phase $LaMnO_3$ are denoted by Miller indices.

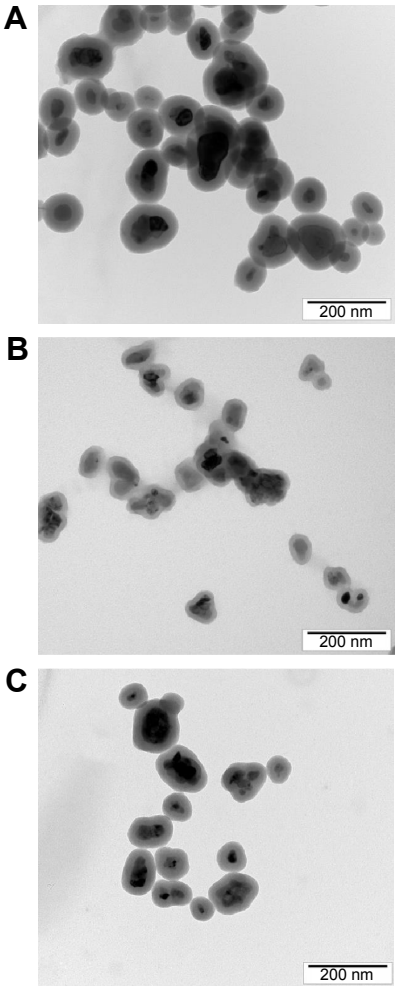

Figure 2 Transmission electron micrograph of the products.
Notes: I: $La_{0.75}Sr_{0.25}MnO_3$, core size 32 nm, silica layer 29 nm (**A**); II: $La_{0.7}Sr_{0.3}MnO_3$, core size 27 nm, silica layer 16 nm (**B**); III: $La_{0.65}Sr_{0.35}MnO_3$, core size 22 nm, silica layer 23 nm (**C**).

Table 2 TEM analysis of silica-coated nanoparticles

Batch no	Composition (x)	$\bar{d}_c$ (nm)	$\bar{d}_p$ (nm)	$\bar{e}$ (nm)
I	0.25	43±21	101±23	29±2
II	0.30	46±19	79±20	16±5
III	0.35	50±21	96±22	23±2

Notes: $\bar{d}_c$, $\bar{d}_p$, and $\bar{e}$ are the (number-averaged) mean diameters of magnetic cores, whole silica-coated nanoparticles, and the mean thickness of silica shell, respectively. Average values are presented with standard deviations.
Abbreviation: TEM, transmission electron micrograph.

other products (I and II) was not measured; however, r_2 was expected even higher due to their bigger core, which was also reflected by higher magnetization.

Magnetic fluid hyperthermia on cell suspensions in vitro

In vitro experiment confirmed the capability of the NPs to heat the cell suspension with high NP concentration and cause cell death. Figure 5 shows substantial temperature increase in the sample containing suspension of AT-MSCs mixed with NPs at high concentration (product III) during exposure to the HF field. The temperature of the sample reached 48.6°C after 1 hour exposure at concentrations 16 mM (Mn). On the contrary, temperature increase in the sample containing pure cell suspension was incomparably lower. Similar results were obtained for other cell types. The reached temperature in case of cells mixed with NPs represents equilibrium between heating power of the suspended NPs and heat loss which increases with increasing sample temperature. It remained ~20°C below Curie temperature, and despite variations in T_c, reached temperature varied within small interval of 47.8°C–48.6°C for all the three products.

Viability of the cells without NPs (both exposed and unexposed to the HF field) reached 90%–100%. Sample handling therefore had a negligible effect on cell viability. Viability of the cells in suspensions with NPs substantially decreased after exposure to the HF field (Table 4). Increase of the temperature caused by magnetic loses during exposure

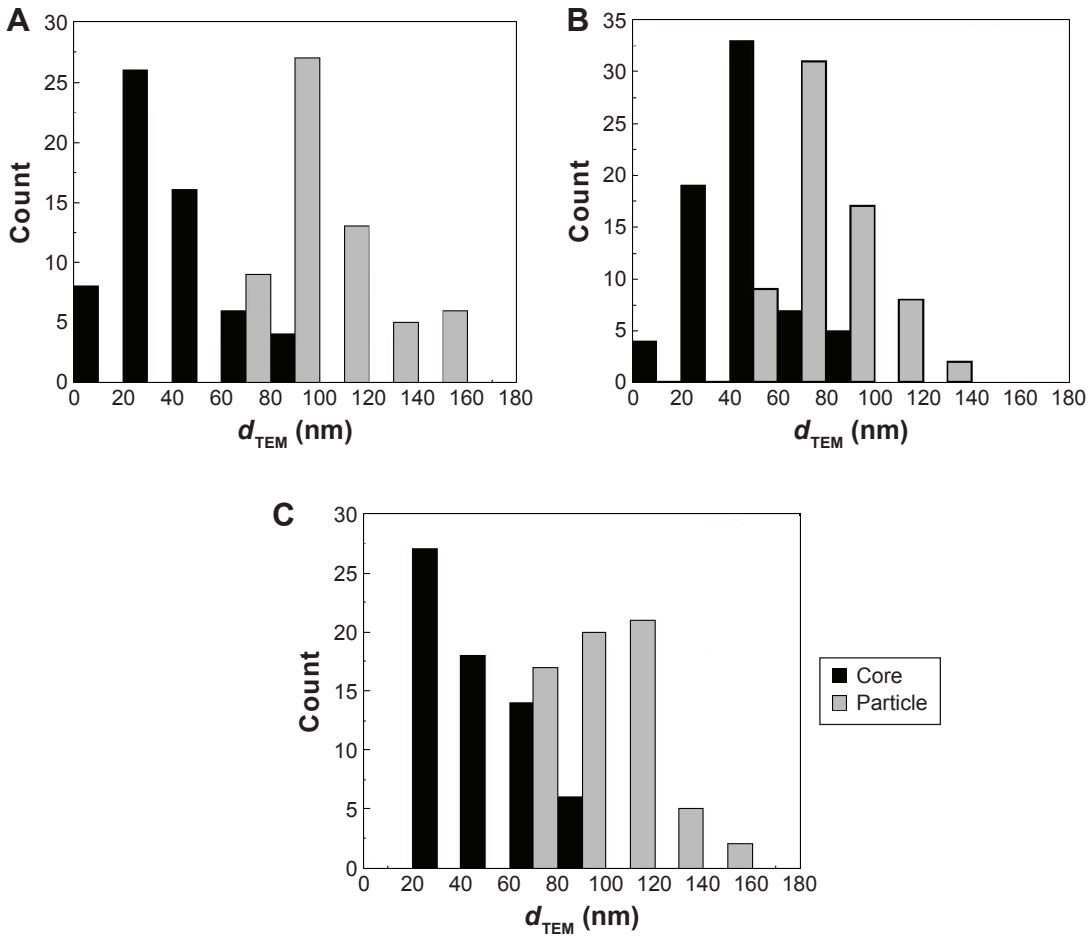

Figure 3 Size distribution histograms of silica-coated nanoparticles.
Notes: (**A**) I, x=0.25; (**B**) II, x=0.30; (**C**) III, x=0.35. The size of magnetic cores (core) and whole silica-coated nanoparticles (particle) are provided as evaluated from TEM data.
Abbreviation: TEM, transmission electron micrograph.

Table 3 Physical properties of the tested $La_{1-x}Sr_xMnO_3$ nanoparticles

Batch no	Composition (x)	Magnetization (@1T) of the uncoated product (Am^2/kg)	Magnetization (@1T) of the coated product (Am^2/kg)	Curie temperature T_c (K)
I	0.25	29.74	6.03	339
II	0.30	24.4	14.5	341
III	0.35	22.6	6.64	346

to the alternating field led to the immediate destruction of a portion of the cells; further decrease of cell viability 24 hours after exposure probably reflects a process of apoptosis initiated by the magnetic field thermoablation.

The NPs had substantial influence on the viability of cells even in samples unexposed to the magnetic field. Although viability 1 hour after NP addition is rather high (80%–97%), it substantially decreased after 24 hours, which means that the NPs at high concentrations during long exposure are toxic for the cells. It should be noted that cells were left in the NP suspension during the 24-hour period; due to high NP concentration, we were not able to wash the NPs out without losing the cells.

The substantial differences in the number of viable cells in different cell types may reflect the different sensitivity of the cells to magnetic fluid hypethermia. Nevertheless, it should be noted that the high concentration of the NPs in the cell suspensions made viability evaluation extremely difficult. Automated cell counters often failed to provide reproducible values due to the presence of NPs in the cell suspensions (which often adhered to the cell surface). Manual counting in a Burker chamber was found to be the most reliable counting method.

MRI

Due to their high r_2 relaxivity, the NPs serve as a good negative contrast agent, which manifested itself as a signal loss in MR images. At high concentrations, the effect of local field inhomogeneities caused by NP suspension injected into the tissue in vivo is so strong, that it may even cause image distortions. Distribution of the NPs in the tumor after injection can therefore be easily verified using MRI (Figure 6). If used for imaging only, the high relaxivity of the NPs would enable a substantial decrease of NP concentration. Therefore, we presume that the adverse effects (cellular toxicity observed at extremely high concentrations) would be negligible.

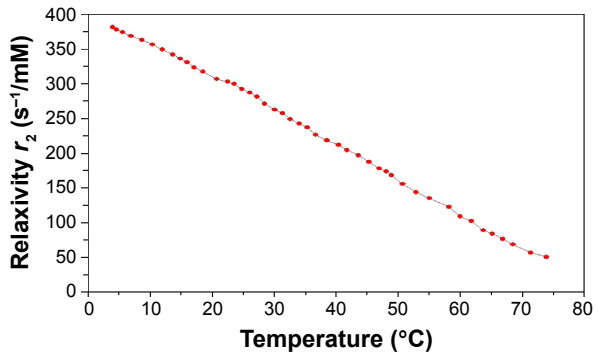

Figure 4 Temperature dependence of the relaxivity r_2 of the $La_{1-x}Sr_xMnO_3$ particles; product III ($La_{0.65}Sr_{0.35}MnO_3$).

Ablation in vivo

One hour exposure to the HF field was a considerable burden for the rats. Substantial increase of body temperature was recorded even in the case of animals without applied NPs, although the temperature in the chamber was kept in the interval of 30°C–32°C.

Figure 7A shows the evolution of the temperature in the tumor during exposure to the HF field. The mean temperature in animals treated by injected NPs increased to 42.9°C±0.6°C; however, control animals without particles reached a similar temperature (42.6°C±0.6°C). Statistical test did not reveal any difference in temperature in the course of ablation. We also found no differences in the observed

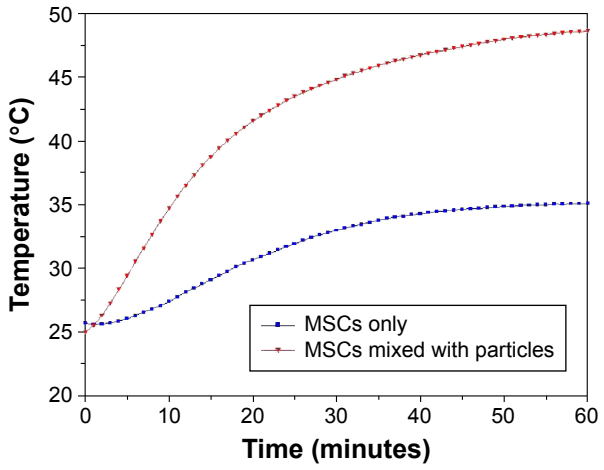

Figure 5 Temperature in the cell suspensions (AT-MSCs) during exposure to the external high-frequency magnetic field.
Notes: Blue – control sample containing MSCs only; red – mixture of MSCs with the nanoparticle suspension (product III).
Abbreviations: AT-MSCs, mesenchymal stem cells from adipose tissue; MSCs, mesenchymal stem cells.

Table 4 Viability of the cells mixed with nanoparticles after magnetic fluid hyperthermia (exposed samples) or 1 hour after addition of the nanoparticles (control samples)

Cell type	Viability immediately after MFH (%)		Viability 24 hours after MFH (%)	
	Exposed sample	Control sample	Exposed sample	Control sample
C6	51	97	45	80
AT-MSCs	0	81	0	38
BM-MSCs	46	96	26	59

Abbreviations: MFH, magnetic fluid hyperthermia; AT-MSCs, mesenchymal stem cells from adipose tissue; BM-MSCs, mesenchymal stem cells from bone marrow.

temperature evolution. Nonparametric Mann–Whitney *U*-test did not reveal any difference in the parameters of the fitted polynomial curve. The experiment thus confirmed that the effect of injected NPs is in vivo very small.

Negligible differences in tumor temperature between treated and untreated animals proved that the deposited power from the NPs is too small and that thermoregulation of the animals is sufficient to conduct the heat away. The role of active thermoregulation was confirmed by the accidental death of one animal during ablation, which resulted in a faster temperature increase (Figure 7B).

Histology

Apoptosis is a natural phenomenon present in tumor cells and was observed to be spread throughout the tumor tissue heterogeneously, extending beyond the central necrosis. Moreover, the level of programmed cell death strongly depends on the tumor size. Therefore, we selected tumors of an adequate size and assessed the comparable regions of the tumors. TUNEL labeling and caspase-3 activation did not reveal substantially higher apoptosis in NP-treated animals after ablation compared with controls. The expressed apoptotic markers were similar in all four groups (animals with NPs treated by the HF magnetic field, untreated animals with NPs, HF-treated animals without NPs, and in untreated controls with implanted tumors; see Figure 8), and their numbers were negligible, taking into consideration the size of the tumor (the numbers differ within all experimental groups from 26 to 115 apoptotic cells per 1 mm^2 of tumor tissue). Statistical comparison is due to negligible numbers of apoptotic markers in all the experimental animals pointless. Histology thus confirmed the ineffectiveness of the treatment using NPs with a low Curie temperature, that is, with low heating power.

The idea of utilizing thermosensitive ferromagnetic materials with a low Curie temperature is not new. Successful experiments were performed with ferromagnetic particles with 100 μm diameter.[22] Their size and magnetic properties ensured sufficient heating to T_c (43°C) within several minutes both in vitro and in vivo in an animal model. The particle size still enables direct injection; however, it cannot be targeted to the tumor by cellular carriers. Copper–nickel NPs (<100 nm)

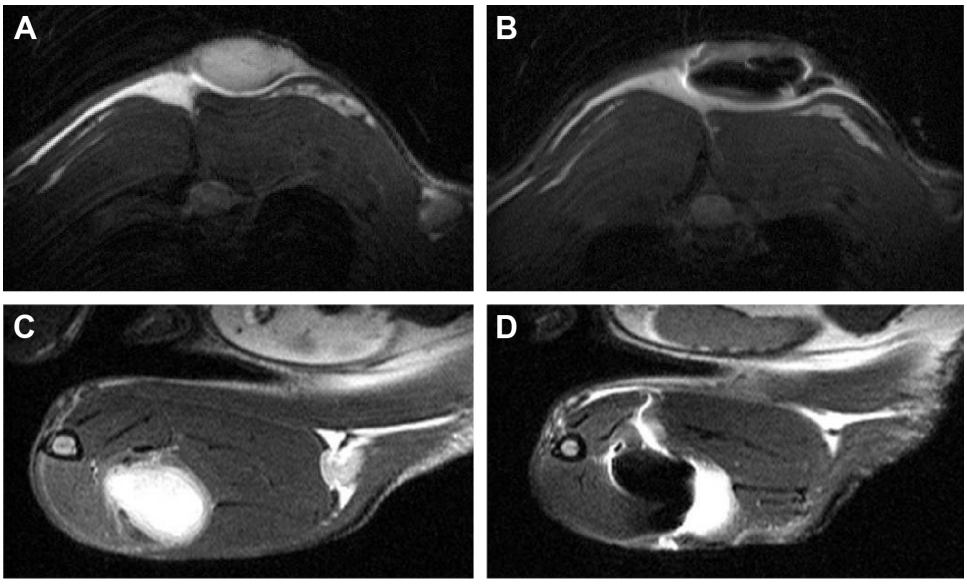

Figure 6 In vivo MRI of a tumor in the rat.
Notes: (**A** and **B**) Axial images of the tumor on the back 2 weeks after subcutaneous injection of the tumor cells; (**C** and **D**) tumor in the hind leg 2 weeks after tumor cell injection. (**A** and **C**) Native MRI before injection of the nanoparticle suspension; (**B** and **D**) MRI after direct injection of the NP suspension into the tumor.
Abbreviation: MRI, magnetic resonance imaging.

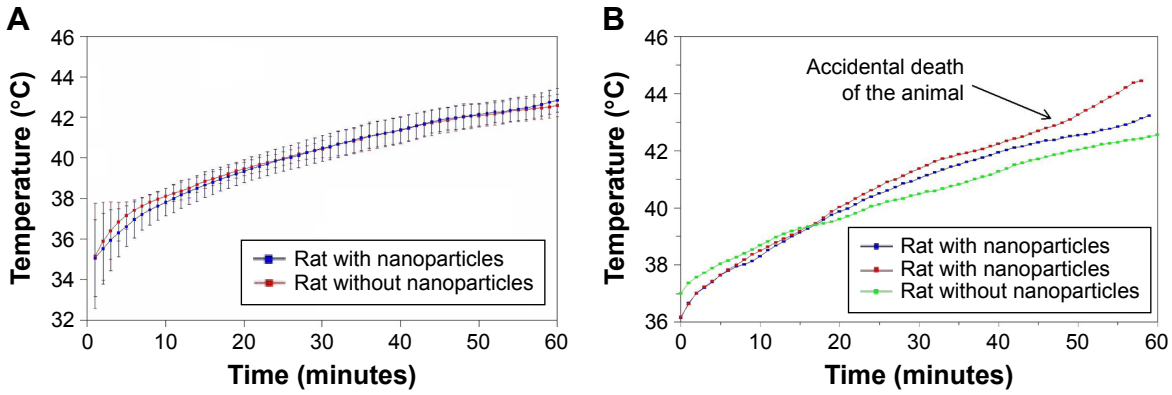

Figure 7 Temperature increase in the tumor during thermoablation.
Notes: Insignificant increase of temperature was observed in the case of animals with applied nanoparticles compared with control rats without nanoparticles. Averaged data with standard deviations are shown (**A**). Higher increase of temperature was observed only in the case of an animal that accidentally died during the experiment; thus, its body temperature was not actively controlled by inherent thermoregulation (**B**).

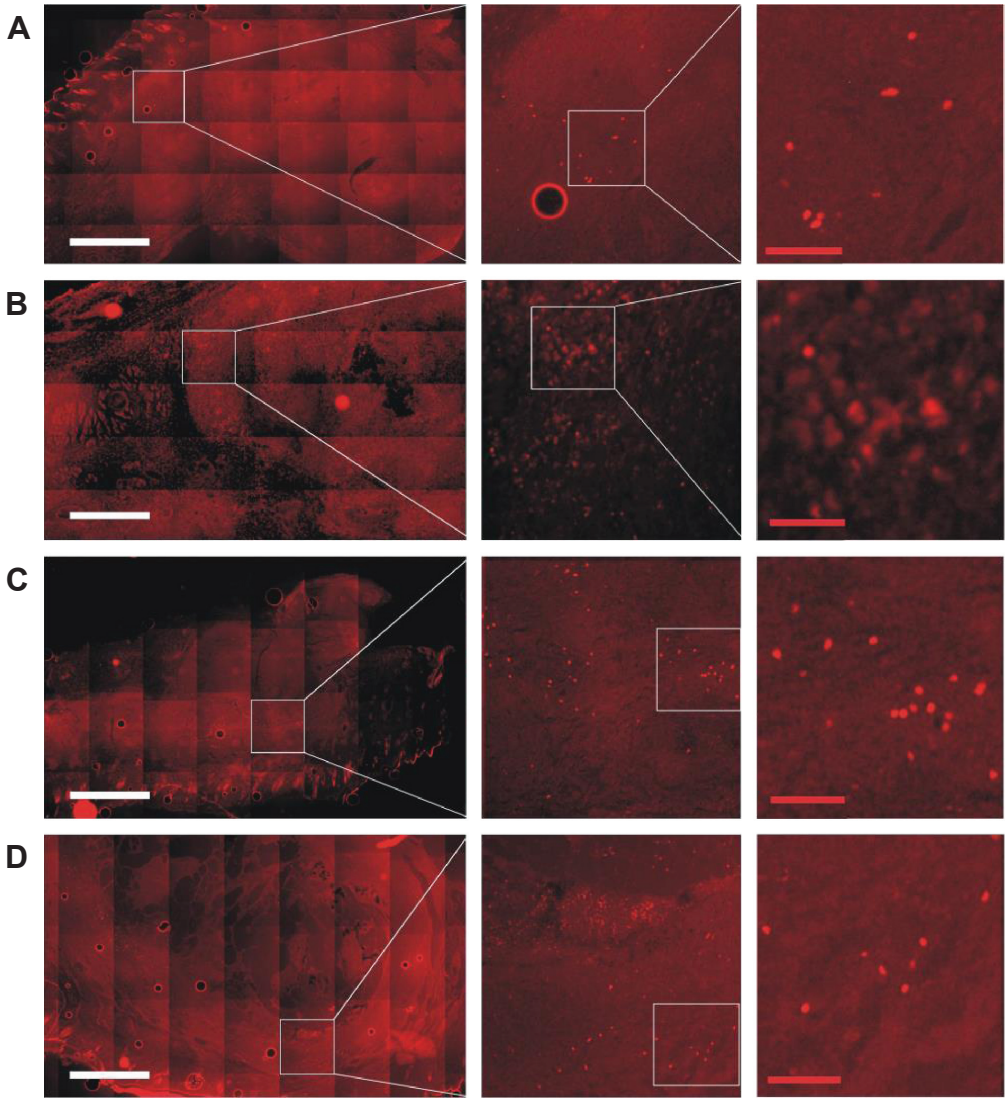

Figure 8 (*Continued*)

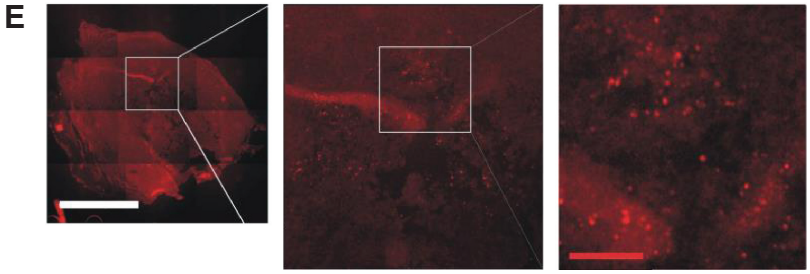

Figure 8 C6 tumors in treated animals.
Notes: (**A**) An animal with nanoparticles injected to the tumor and exposed to the HF field; caspase-3 activation. (**B**) Same animal; terminal deoxynucleotidyl transferase dUTP nick end labeling (TUNEL). (**C**) A control untreated animal without nanoparticles; caspase-3 activation. (**D**) A control untreated animal with injected particles; caspase-3 activation. (**E**) A control animal exposed to the HF without injected particles; caspase-3 activation. White scale bar: 1 mm, red scale bar: 50 μm. Histology revealed no substantial changes in apoptotic markers in the tumor between animals with and animals without injected nanoparticles, similarly no changes were found between animals treated (exposed to the HF field) and untreated ones.
Abbreviations: TUNEL, transferase dUTP nick end labeling; HF, high frequency.

with T_c =40°C–60°C were tested by Kuznetsov et al.[23] They proved that the tissue may be heated by the deposited NPs, nevertheless long-term biocompatibility of the particles is questionable due to missing coating. The silica layer, which we used as a NP coating, should be thick enough to prevent direct contact of the core with the environment in vivo and may ensure safeness of the material. However, usage of the coating substantially limits the core size and its magnetization. Although Curie temperature can be set by the ratio of La and Sr in the core within the required interval (45°C–75°C), due to low magnetization the heating power is insufficient to initiate apoptosis in the tissue.

Conclusion

It was proved that silica-coated LSMO ferromagnetic NPs with a low Curie temperature can be used as a contrast agent. They are efficient due to their high relaxivity, which enables lower doses to be used than in the case of iron oxide NPs. Lower doses may minimize possible toxic effects, which may be further decreased by improving the silica coating. The NPs can be heated by an alternating HF field. Selected LSMO particles with suitable physical and chemical properties are capable of inducing cell apoptosis and cell death in vitro provided they are in sufficient concentration. However, their effect in the case of extracellular deposition in vivo is questionable, due to low deposited power and efficient thermal regulation in living recipients.

Acknowledgments

The financial support of the Ministry of Industry and Trade (grant project TIP FR-TI3/521), the Ministry of Health of the Czech Republic (Institute for Clinical and Experimental Medicine – IKEM, Project IN 00023001), and the Ministry of Education, Youth and Sports of the Czech Republic (Institute of Experimental Medicine AS CR, project LO1309) is gratefully acknowledged.

This paper was presented in part at the World Molecular Imaging Congress 2014, September 17–20, 2014, Seoul, Korea, as a poster presentation with interim findings. The abstract of the poster was published in *Mol Imaging Biol*. 2015;17(Suppl 1):P366 (DOI: 10.1007/s11307-014-0809-1). The actual paper, however, has never been published.

Disclosure

Vít Herynek and Pavel Veverka are co-originators of a Czech patent No 301005 "Process for preparing hybrid nanoparticles from nanoparticle agglomerates of complex multicomponent metal oxides" (2009). The authors report no other conflicts of interest in this work.

References

1. Torres-Lugo M, Rinaldi C. Thermal potentiation of chemotherapy by magnetic nanoparticles. *Nanomedicine*. 2013;8(10):1689–1707.
2. Cheng Y, Morshed RA, Auffinger B, Tobias AL, Lesniak MS. Multifunctional nanoparticles for brain tumor imaging and therapy. *Adv Drug Deliv Rev*. 2014;66:42–57.
3. Palazzi M, Maluta S, Dall'Oglio S, Romano M. The role of hyperthermia in the battle against cancer. *Tumori*. 2010;96(6):902–910.
4. Verma J, Lal S, Van Noorden CJF. Nanoparticles for hyperthermic therapy: synthesis strategies and applications in glioblastoma. *Int J Nanomedicine*. 2014;9(1):2863–2877.
5. Kossatz S, Ludwig R, Dahring H, et al. High therapeutic efficiency of magnetic hyperthermia in xenograft models achieved with moderate temperature dosages in the tumor area. *Pharm Res*. 2014;31(12):3274–3288.
6. Hilger I, Hiergeist R, Hergt R, Winnefeld K, Schubert H, Kaiser WA. Thermal ablation of tumors using magnetic nanoparticles – an in vivo feasibility study. *Invest Radiol*. 2002;37(10):580–586.
7. Duguet E, Vasseur S, Mornet S, Devoisselle JM. Magnetic nanoparticles and their applications in medicine. *Nanomedicine*. 2006;1(2):157–168.
8. Rosensweig RE. Heating magnetic fluid with alternating magnetic field. *J Magn Magn Mater*. 2002;252(1–3):370–374.
9. Pankhurst QA, Connolly J, Jones SK, Dobson J. Applications of magnetic nanoparticles in biomedicine. *J Phys D Appl Phys*. 2003;36(13):R167–R181.

10. Pankhurst QA, Thanh NTK, Jones SK, Dobson J. Progress in applications of magnetic nanoparticles in biomedicine. *J Phys D Appl Phys*. 2009;42(22):224001.
11. Mornet S, Vasseur S, Grasset F, et al. Magnetic nanoparticle design for medical applications. *Prog Solid State Chem*. 2006;34(2–4):237–247.
12. Pollert E, Knizek K, Marysko M, Kaspar P, Vasseur S, Duguet E. New T-c-tuned magnetic nanoparticles for self-controlled hyperthermia. *J Magn Magn Mater*. 2007;316(2):122–125.
13. Pollert E, Kaman O, Veverka P, et al. Core-shell $La_{1-x}Sr_xMnO_3$ nanoparticles as colloidal mediators for magnetic fluid hyperthermia. *Phil Trans R Soc A*. 2010;368(1927):4389–4405.
14. Pollert E, Kaspar P, Zaveta K, Herynek V, Burian M, Jendelova P. Magnetic nanoparticles for therapy and diagnostics. *IEEE Trans Magn*. 2013; 49(1):7–10.
15. Kaman O, Veverka P, Jirak Z, et al. The magnetic and hyperthermia studies of bare and silica-coated $La_{0.75}Sr_{0.25}MnO_3$ nanoparticles. *J Nanopart Res*. 2011;13(3):1237–1252.
16. Veverka M, Zaveta K, Kaman O, et al. Magnetic heating by silica-coated Co-Zn ferrite particles. *J Phys D Appl Phys*. 2014;47(6): 65503–65513.
17. Jendelova P, Herynek V, DeCroos J, et al. Imaging the fate of implanted bone marrow stromal cells labeled with superparamagnetic nanoparticles. *Magn Reson Med*. 2003;50(4):767–776.
18. Fabryova E, Jirak D, Girman P, et al. Effect of mesenchymal stem cells on the vascularization of the artificial site for islet transplantation in rats. *Transplant Proc*. 2014;46(6):1963–1966.
19. Zvatora P, Veverka M, Veverka P, et al. Influence of surface and finite size effects on the structural and magnetic properties of nanocrystalline lanthanum strontium perovskite manganites. *J Solid State Chem*. 2013; 204:373–379.
20. Babic M, Horak D, Trchova M, et al. Poly(L-lysine)-modified iron oxide nanoparticles for stem cell labeling. *Bioconjugate Chem*. 2008;19(3): 740–750.
21. Horak D, Babic M, Jendelova P, et al. D-Mannose-modified iron oxide nanoparticles for stem cell labeling. *Bioconjugate Chem*. 2007;18(3): 635–644.
22. Saito H, Mitobe K, Ito A, et al. Self-regulating hyperthermia induced using thermosensitive ferromagnetic material with a low Curie temperature. *Cancer Sci*. 2008;99(4):805–809.
23. Kuznetsov AA, Leontiev VG, Brukvin VA, et al. Local radiofrequency-induced hyperthermia using CuNi nanoparticles with therapeutically suitable Curie temperature. *J Magn Magn Mater*. 2007;311(1): 197–203.